PERGAMON

Journal of Structural Geology 21 (1999) 1731–1749

JOURNAL OF STRUCTURAL GEOLOGY

www.elsevier.nl/locate/jstrugeo

Strike-slip fault-propagation cleavage in carbonate rocks: the Mattinata Fault Zone, Southern Apennines, Italy

Francesco Salvini[a,*], Andrea Billi[a], Donald U. Wise[b]

[a]*Dipartimento di Scienze Geologiche, Università Roma Tre, Largo S. L. Murialdo 1, 00146 Rome, Italy*
[b]*Department of Geosciences, Franklin and Marshall College, P.O. Box 3003, Lancaster, PA 17604-3003, USA*

Received 2 July 1998; accepted 8 June 1999

Abstract

Disjunctive, spaced solution cleavage in carbonate rocks is genetically associated with the propagation of the left-lateral, strike-slip Mattinata Fault in the Gargano Promontory, Italy. Typical cleavage development is restricted within the 200–300-m-wide fault zone, which is bounded by virtually unfractured wall rocks. The cleavage consists of sub-parallel solution surfaces, which are often reactivated as sheared solution planes. Geometrical and kinematic relationships exist between the fault and the associated cleavage planes, thus: (1) cleavage–fault intersection lines lie parallel to the fault and the sheared cleavage rotational axes and (2) the cleavage–fault angle is almost constantly equal to 40°. A model for the development of the Mattinata Fault is proposed in which the cleavage surfaces are interpreted as fault-propagation deformations. Cleavage nucleates as solution planes at the front of the advancing fault as the result of stress concentration in this region. Two distinct, time-sequential processes are shown to operate during the fault propagation: (1) typical millimetre- to centimetre-spaced solution surfaces form in the distal tip zone of the advancing fault plane; (2) as the tip advances, the fault plane breaks through the cleavage as minor shear displacements reactivate some of these nascent surfaces. These observations may prove useful in understanding mechanisms for fault-controlled enhanced/reduced permeability and fluid pathways.

1. Introduction

The role of pressure solution in cleavage formation has been widely recognised in different tectonic and lithological environments in the work of several authors (Sharpe, 1847; Sorby, 1853, 1856; Nickelsen, 1972; Groshong, 1975; Alvarez et al., 1976; Mitra et al., 1984; Marshak and Engelder, 1985). Somewhat uniformly spaced but irregular and locally stylolitic surfaces with residues of insoluble materials are now regarded as the hallmarks of the pressure solution creation process (Stockdale, 1922; Dunnington, 1954; Park and Schot, 1968; Guzzetta, 1984). The generally accepted origin is from maximum shortening parallel to the stylolite teeth (Dieterich, 1969; Carannante and Guzzetta, 1972; Siddans, 1972) with a time frame slow enough for operation of the chemical processes of solution, transport and redeposition (Weyl, 1959; Rutter, 1976, 1983; Groshong, 1988; Andrews and Railsback, 1997). Even though these mechanisms occur in a fault zone, the chemical time constraint excludes formation as an instantaneous co-seismic event (Gratier and Gamond, 1990).

Solution surfaces/cleavages can develop comparatively uniformly across significant parts of orogenic zones (Illies, 1975; Bell, 1978; Illies and Greinier, 1978, 1979; Engelder and Geiser, 1979; Odom et al., 1980; Mitra et al., 1984; Marshak and Engelder, 1985; Mitra and Yonkee, 1985; Ohlmacher and Aydin, 1995) or as planes of localised development in association with folds (Choukroune, 1969; Alvarez et al., 1976; Henderson et al., 1986) and/or faults (Arthaud and Mattauer, 1969; Rispoli, 1981; Gaviglio, 1986; Nickelsen, 1986; Pollard and Segall, 1987; Aydin, 1988; Hyett, 1990; Ohlmacher and Aydin, 1995, 1997; Peacock and Sanderson, 1995a, b; Petit and Mattauer,

* Corresponding author.
E-mail address: salvini@uniroma3.it (F. Salvini)

0191-8141/99/$ - see front matter
PII: S0191-8141(99)00120-0

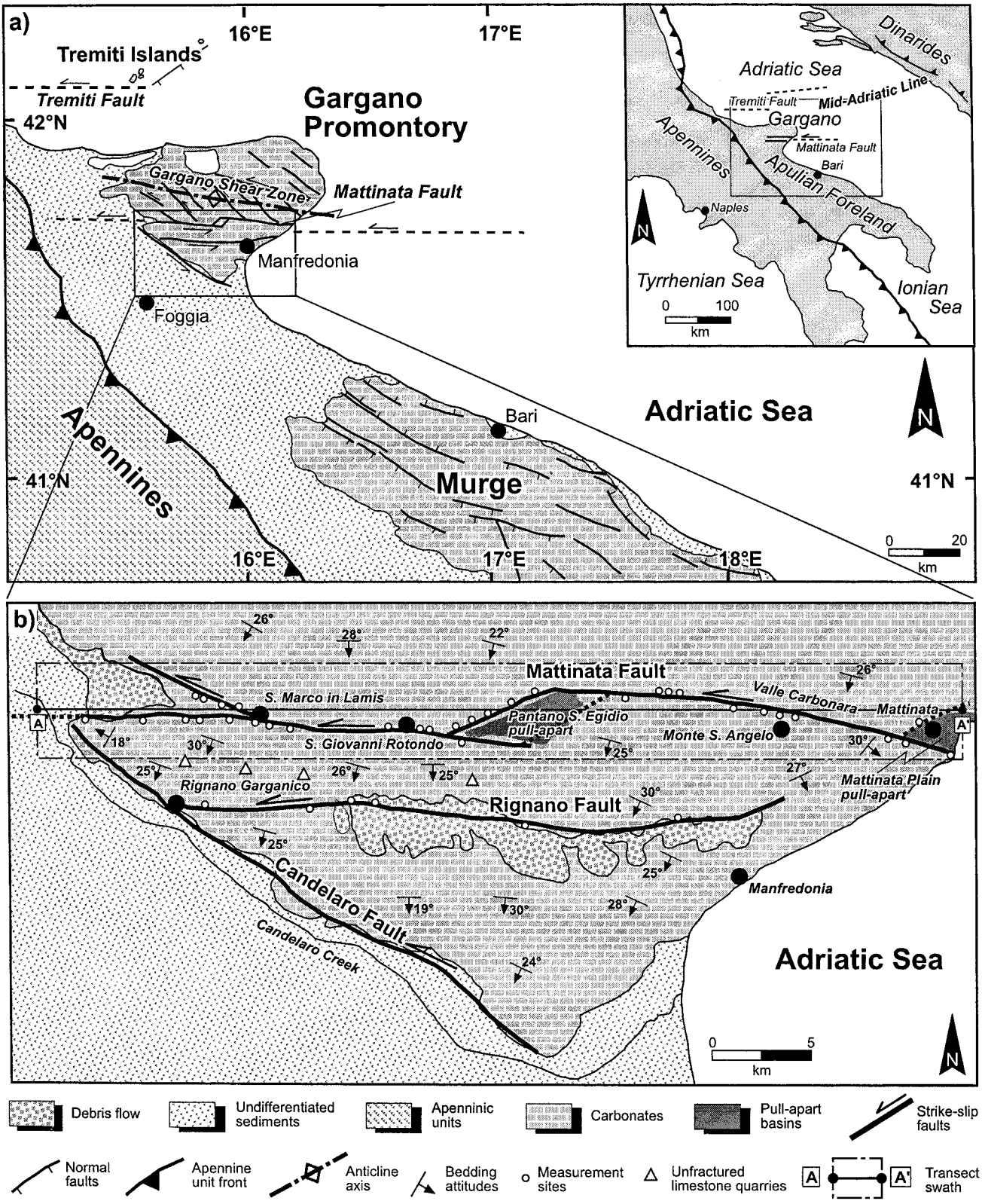

Fig. 1. Index maps. (a) Geological map of the Mid-Adriatic Region. Square inset shows the geodynamic framework of Southern Italy. (b) Geological map of the study area.

1995; Willemse et al., 1997; Kelly et al., 1998; Peacock et al., 1999). Mechanisms associated with the near-tip stress of advancing faults are increasingly recognised as significant factors in the development of solution surfaces (Gaviglio, 1986; Pollard and Segall, 1987; Aydin, 1988; McGrath and Davison, 1995; Petit and Mattauer, 1995; Homberg et al., 1997; Ohlmacher and Aydin, 1997). Since the work of Griffith (1924), it has been shown that sliding on a pre-existing flaw leads to a concentration of the stress around the growing flaw. The near-tip stress concentration may generate dilation cracks (i.e. wing cracks or tail cracks, *sensu* Brace et al., 1966 and Cruikshank et al., 1991) which normally occur in the tensile quadrants, at a sharp angle from the sliding flaw (Pollard and Segall, 1987). Wing cracks have been also shown to emanate from one or both ends of the planar flaw loaded in shear in brittle homogeneous isotropic materials during experimental studies (Sheldon, 1912; Brace and Bambolakis, 1963; Erdogan and Sih, 1963; Hoek and Beniawski, 1965; Nemat-Nasser and Horii, 1982; Horii and Nemat-Nasser, 1985, 1986; Ashby and Hallam, 1986). In some materials, such as carbonate rocks, in addition to wing cracks, the near-tip stress concentration may also alternatively generate solution surfaces which occur on the opposite, contracting quadrants (Arthaud and Mattauer, 1969; Rispoli, 1981).

A number of researchers have dealt with the kink angle of wing cracks and solution surfaces and their tendency for near-tip nucleation (Irwin, 1957; Ida, 1972; Cotterell and Rice, 1980; Pollard and Segall, 1987; Cox and Scholz, 1988; Petit and Barquins, 1988; Aydin and Schultz, 1990; Reches and Lockner, 1994; Petit and Mattauer, 1995; Cooke and Pollard, 1996; Cooke, 1997; Martel, 1997; Willemse, 1997; Willemse et al., 1997; Willemse and Pollard, 1998), providing different solutions according to specific boundary conditions and to specific adopted mechanical theories. As well as the opposite tensile/compression stress concentrations at the fault tip sides, sliding along a pre-existing fault also generates a region of increased stress which extends from the fault tip to the region just ahead of it (Chinnery, 1963; Pollard and Segall, 1987; King et al., 1994). The stress concentration is responsible for the propagation of the fault surface by shearing. With progressive increase of the stress, the unfaulted rock in front of the fault plane is elastically distorted until the rock strength is overcome and the rupture propagates by shear. Experiments have shown that the size of the region of the increased stress ahead of the tip scales with the fault width (Pollard and Segall, 1987; Lyakhovsky et al., 1997) and linearly with the fault length (Chernyshev and Deanman, 1991; Scholz et al., 1993; Reches and Lockner, 1994). As a consequence, deformations deriving from the stress concentration in the near-tip zone may affect a larger region when associated with the propagation of a regional size fault (Reches and Lockner, 1994).

In our paper, we propose that this strain mechanism operated at the advancing front of the Mattinata Fault in the Gargano Promontory (Fig. 1), Italy, to generate localised solution-based fault-propagation cleavage. The genetic process considered here differs substantially from simple wing cracking mechanisms.

The cleavage analysed in this paper is restricted to those carbonate rocks of the Gargano Promontory lying within a 200–300-m-wide zone of deformation associated with the regional, left-lateral, strike-slip Mattinata Fault (Funiciello et al., 1988) and some of its adjoining faults (Fig. 1). No cleavages are found outside the fault zones. These faults are part of the E–W-trending mid-Adriatic Line defined by abrupt changes in morphological, structural and seismic features within the Adriatic Sea (Favali et al., 1993a, b). The Line represents a roughly E–W kinematic boundary across the Adriatic domain, extending from the Tremiti Fault and the Tremiti Islands in the north to several faults of the Gargano Promontory in the south (Fig. 1).

The well-exposed Mattinata Fault within the Meso-Cenozoic carbonate rocks of the Gargano Promontory was used to analyse cleavage features and cleavage spatial distribution within a fault zone. Comparisons were made with the cleavage population sampled along the adjacent Rignano Fault (Fig. 1).

The aim of this paper is to show that within regional fault zones in carbonate rocks, cleavage surfaces may have a distribution which derives from concentration of the stress within the virgin rock at the front of the propagating fault tip. The studied cleavage differs from the *S*-planes of Berthé et al. (1979) by the broader scale at which it forms and by the brittle or semi-brittle (*sensu* Davis and Reynolds, 1996) nature of the shear zone to which it is associated.

The model of development of cleavages within the Mattinata Fault relies on a field-based fault zone characterisation. The Mattinata Fault is exposed for a few tens of kilometres within thick carbonate successions. A series of exposures along the fault provide a rather detailed but discontinuous record of the fault zone-related deformations. A specific method of automated data processing (see Appendix) helped in solving the problem of spatially analysing data gathered at discrete discontinuous sites along a regional fault.

We analyse the cleavage sets of the Mattinata Fault and establish a number of geometrical and kinematic relationships between the fault and the associated cleavage system. The results are compared with those from the adjacent Rignano Fault. Based on these observations, we propose a model for the development of this cleavage as a fault-propagation structure. In ad-

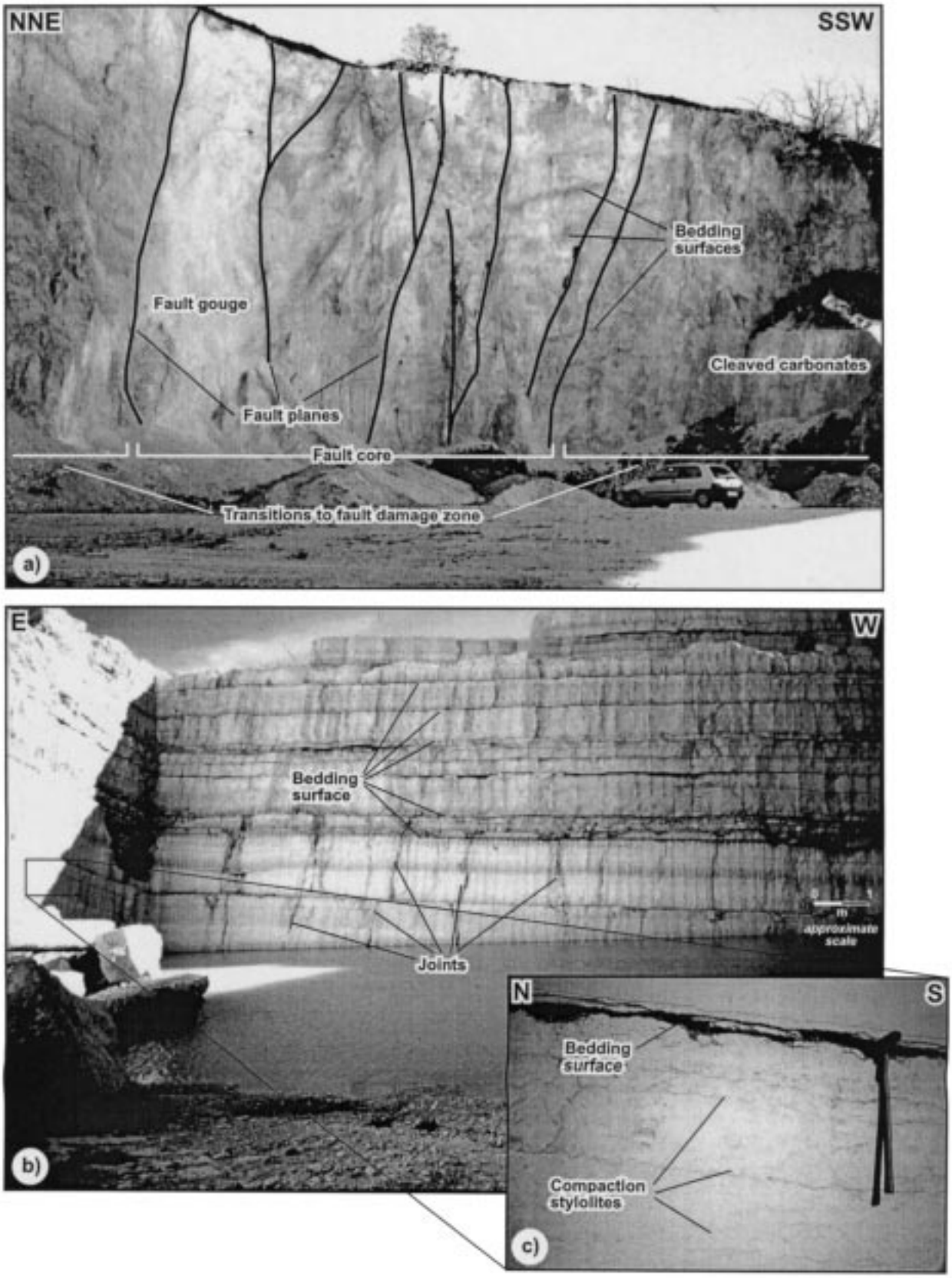

Fig. 2. (a) Photograph of an active quarry wall illustrating a section across the Mattinata Fault Zone (Valle Carbonara). In the photograph, the fault core, characterised by master slip planes encompassed by cataclasites and gouges, can be observed. Within the core, relics of the bedding surfaces are still preserved. (b) Photograph of an abandoned quarry (south of S. Marco in Lamis) illustrating almost unfractured limestone beds belonging to the Mattinata Fault wall rocks. In the quarry, large blocks of undeformed limestone were once obtained. The only obvious structures at this scale are large asystematic joints. (c) Photograph illustrating details of a limestone bed from (b). Stylolitic surfaces parallel to bedding are observable at this scale.

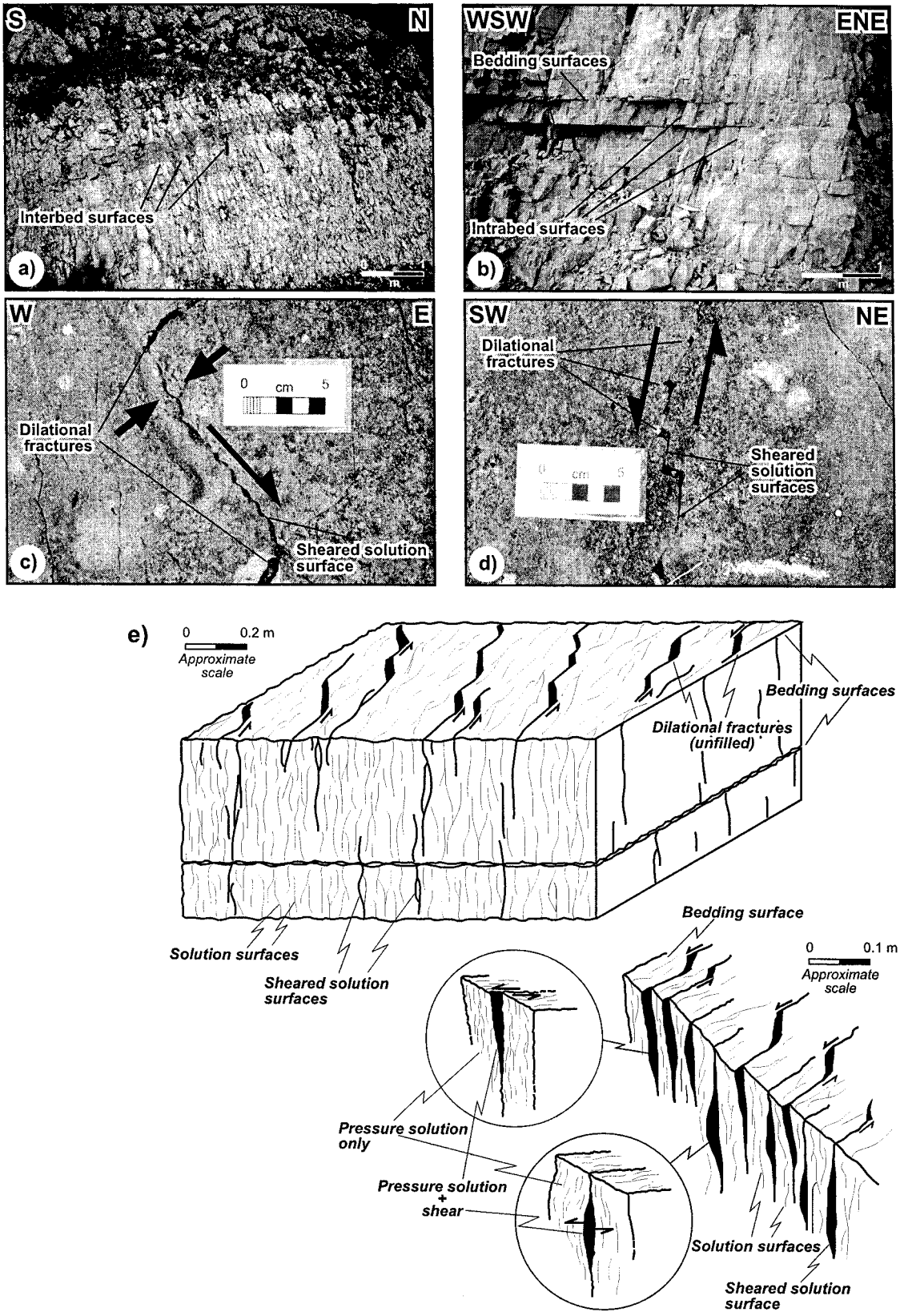

Fig. 3. Photographs and block diagrams showing cleavages in carbonate rocks. (a) Photograph mostly illustrating interbed cleavage planes cutting across the bedding surface. (b) Photograph mostly illustrating intrabed cleavage planes abutted by bedding surfaces. (c) Photograph illustrating a bedding surface with a NW–SE sutured intersection lineation of a cleavage plane. Note the millimetre right-lateral offset of the teeth and the consistent opening of the NE–SW dilation fractures at the two extensional quadrants of the cleavage tips. Arrows indicate the sense of displacement by pressure solution and shear. (d) Photograph illustrating a bedding surface with a N–S set of échelon cleavage smooth intersection lineations. Note the dilation fractures opening at the cleavage tips, which show a left lateral offset. Arrows indicate the sense of displacement by shear. (e) Block diagrams illustrating the typical pattern of cleavage surfaces affecting carbonate beds. Millimetre- to centimetre-spaced solution surfaces (thinner lines) are contained within lithons bounded by decimetre-spaced sheared solution surfaces (thicker lines). Solution surfaces develop within carbonate layers mostly as intrabed planes, whereas the sheared solution surfaces may propagate across the bedding planes as interbed planes.

dition to throwing some light on fault tip processes, these observations may prove useful in understanding permeability and fluid paths associated with some fault zones in carbonate rocks. The methodology we adopted to quantitatively assess the changing azimuths of the cleavage pattern along strike is dealt with in the Appendix at the end of the paper.

2. The Gargano Promontory

The Gargano Promontory is easily identified as an ENE-elongated prominence along the Italian Adriatic coast (Fig. 1). The promontory is part of the Apulian Platform, the foreland for both the Apennine (Miocene–Pleistocene) and the Dinaride (Eocene–Miocene) thrust and fold belts (Fig. 1a). Its lithology developed in the Adriatic microplate (Biju-Duval et al., 1977; Vandenberg, 1979; Hsü, 1982; Manzoni and Vandenberg, 1982; Funiciello et al., 1991; Favali et al., 1993a, b) as part of the Apulian Mesozoic carbonate shelf along a passive margin of the Tethys Ocean.

The Gargano area is underlain by more than 4000 m of a discontinuous marine carbonate sequence ranging in age from Triassic to Middle Miocene. Prevailing shallow water carbonates crop out in the central and western sectors of Gargano, whereas to the east and northeast such sequences are progressively bounded by Mesozoic carbonate slope and basin deposits (Bosellini et al., 1993 and references therein).

The promontory is a left-lateral, transpression-related, asymmetric, anticlinal high with the axis trending WNW–ESE (Fig. 1a). Mesozoic carbonate formations rise to over 1000 m above sea level in the promontory whereas the same formations reach only 500–600 m in most of the adjacent plains. Dissecting the promontory along its approximate anticlinal hinge is the Gargano Shear Zone, an E–W trending region of left-lateral offset (Fig. 1a) characterised by a pattern of well defined, E–W and NW–SE-trending faults. Minor, local, NW–SE strike-slip related folds are consistent with the left-lateral tectonics. The southern sector of the Gargano Shear Zone is characterised by the presence of three major faults, the E–W Mattinata and Rignano faults, and the WNW–ESE Candelaro Fault, a feature which bounds the SW corner of the uplift (Fig. 1b). This study focuses on the Mattinata Fault located in the south flank of the promontory (Fig. 1b), characterised by carbonate rocks with typical south dips of 20–30°.

The Mattinata Fault is the most prominent member of the Gargano Shear Zone. The fault has an irregular trace characterised by a number of significant morphological features compatible with left-lateral strike-slip tectonics. Proceeding westward from the coastline, these features include the Mattinata plain (Fig. 1b) as a narrow triangular depression formed at a counter-clockwise releasing bend of the main fault. Next, the Valle Carbonara is a gully located at a 20° clockwise bend of the main fault. Westward, the Pantano S. Egidio pull-apart basin (Guerricchio, 1986; Funiciello et al., 1988) forms a shallow rhomb-shaped depression at a left-step of the main fault. Toward the western end, just northwest of the S. Marco in Lamis village (Fig. 1b), a WNW-striking fault branches out from a restraining bend of the main E–W Mattinata Fault to produce a number of outcrop-scale transpressional features.

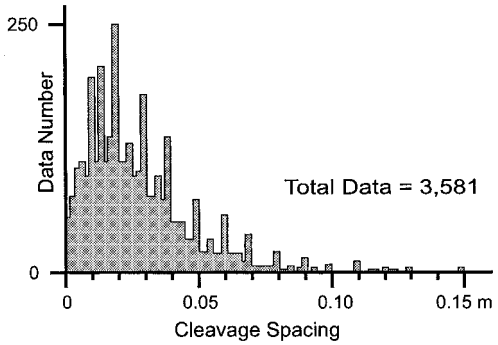

Fig. 4. Histogram of cleavage spacing between adjacent solution or sheared solution planes (see Fig. 5b) from the Mattinata, Rignano and Candelaro fault zones.

3. The Mattinata fault-related cleavage

The cleavage associated with the Mattinata Fault Zone consists of an array of disjunctive, spaced, solution surfaces affecting the carbonate rocks within its entire, exposed fault zone. The Mattinata Fault Zone ranges in width from a few tens of metres to about 300 m and is typically about 200 m wide. Its exposed on-shore length of more than 40 km (Fig. 1) is composed of two contrasting structural fabrics (Fig. 2a): (1) the fault core and (2) the fault damage zone (Caine et al., 1996). The central core occupies 10–20% of its total width. The core includes the master slip surface and associated bands of cataclastic breccias and gouges. Because of cataclasis and extensive rock crushing, cleavage surfaces are rarely detectable in the core zone. Beyond the core, the broader damage zone consists of a network of both sub-parallel and cross-cutting subsidiary slip surfaces breaking through masses of intensely cleaved carbonate rocks. The poorly exposed outer boundaries of the damage zone appear to give out in a few metres to almost undeformed wall rocks (Fig. 2b and c). No cleavages have been found beyond this rather abrupt boundary. Within another few 10s to 100 m from the boundary zone, carbonate rocks are nearly undeformed except for poorly devel-

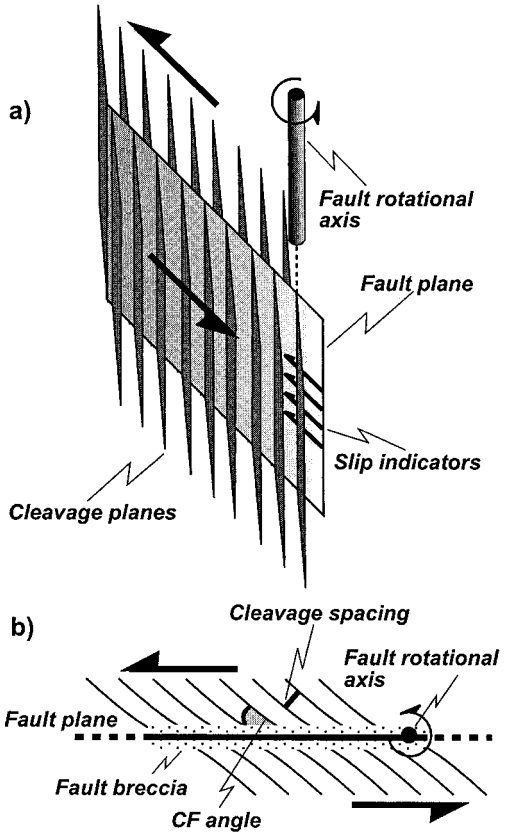

Fig. 5. (a) Three-dimensional sketch illustrating geometrical and kinematic relationships between fault and cleavage planes. The intersection line between the cleavage and the fault planes lies parallel to the fault rotational axis. (b) Map view of (a). Cleavage planes form an acute angle with the fault plane (cleavage–fault, CF angle). In approaching the fault plane this angle decreases with progressive bending of the cleavage planes into closer parallelism with the fault surface. Development of fault breccia along the fault plane generates free boundaries between the fault and the cleavage surfaces.

oped systematic intrabed joints. This spatial contrast is best observed at several quarries located between the Mattinata and Rignano faults south of S. Marco in Lamis and S. Giovanni Rotondo (Fig. 2).

The cleavage surfaces investigated within the Mattinata Fault Zone have nearly vertical dips and a general NW–SE strike (Fig. 3). Their spacing ranges from 0.001 to 0.3 m and from 0.01 to 0.03 m on average (Fig. 4). The spacing of the cleavage surfaces within the carbonate rocks is found to decrease slightly in approaching the fault planes. Stylolites (Fig. 3c) as well as slight truncation of fossils along the cleavage surfaces reveal their dissolution nature. Strike-slip slickolites and/or slickensides along some of the cleavage planes testify to shear displacement along them. Locally on bedding surface exposures, dilation fractures with 0.001–0.03 m opening, emanate from and connect with the tips of closely spaced sheared cleavage planes (Fig. 3c). Some lateral offset of the stylolitic teeth or of serrate profiles observed on bedding surfaces (Fig. 3c) from cleavage intersections suggests that shear processes along the cleavage planes postdate the dissolution. The magnitude of these shear displacements, estimated through the lateral offset of markers or through the aperture of the dilation fractures opening at the cleavage termination, is in the order of 0.001–0.03 m. Adjacent, parallel surfaces can show differing evolutionary development: formation of the plane by simple solution with some planes showing later shearing along the solution surfaces (Fig. 3). Solution surfaces are typically intrabed structures whose development halts top and bottom at bedding planes (Fig. 3b). On the other hand, sheared solution surfaces commonly cut across bedding planes (interbed surfaces in Fig. 3a). Evidence of younger shear displacement is found along a more limited number of the cleavage surfaces with typical spacing of 0.1–1 m. The typical pattern is of 0.001–0.1-m-spaced solution surfaces lying within 0.1–1-m-wide lithons which are

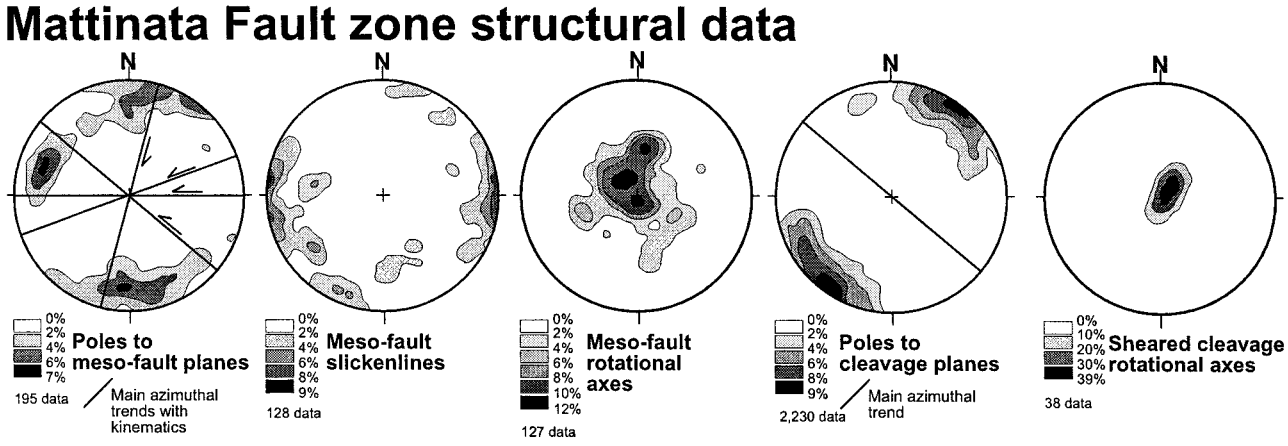

Fig. 6. Contoured stereograms (Schmidt projections, lower hemisphere) of the structural data sampled within the Mattinata Fault Zone.

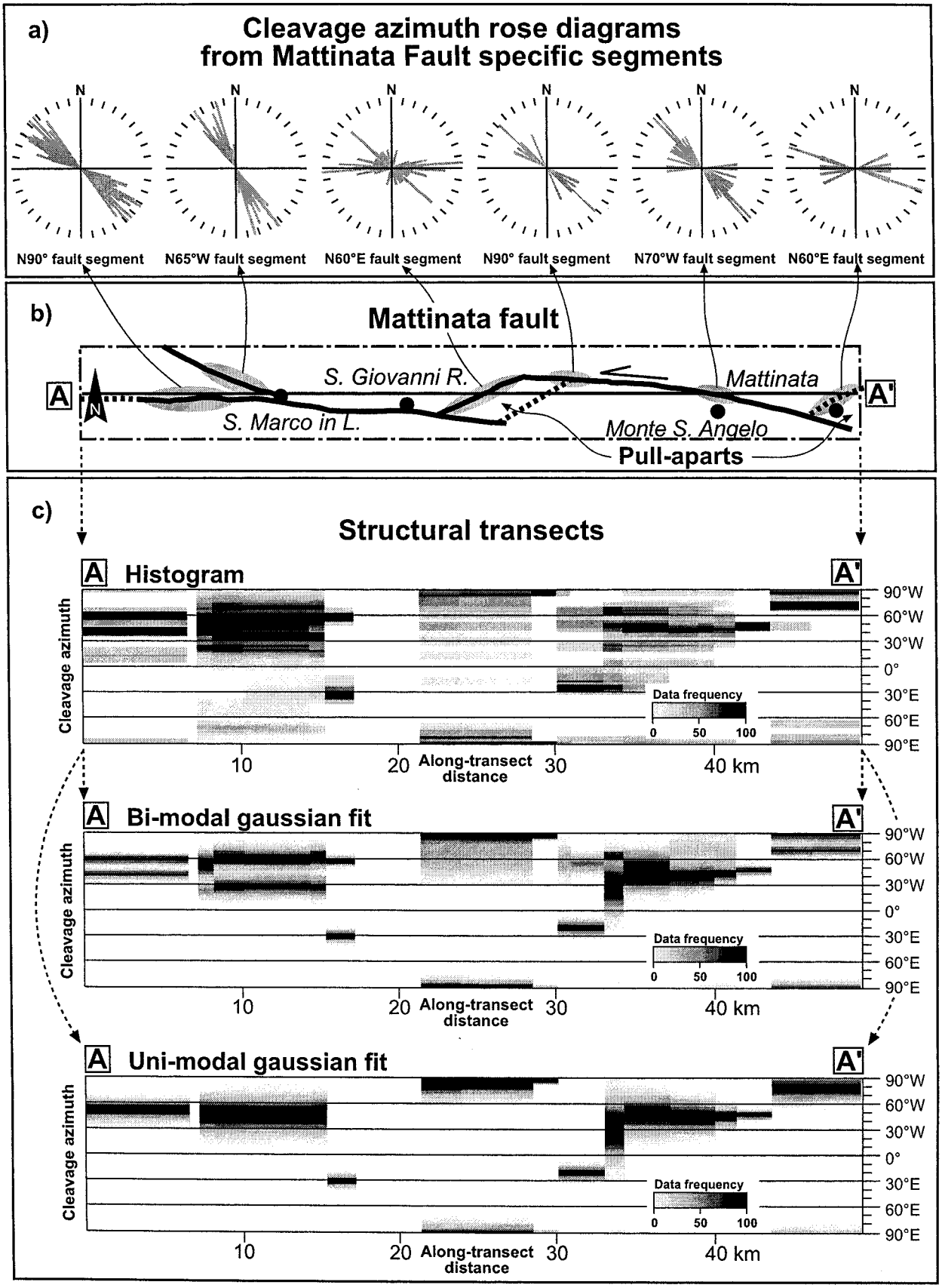

Fig. 7. (a) Rose diagrams showing cleavage azimuths from specific segments of the Mattinata Fault. Arrows indicate areas (shaded in b) of data sampling. (b) Trace of the Mattinata Fault and area (A–A′) along the structural transect swath. (c) Structural transect diagrams representing cleavage azimuth frequency versus distance along the transect swath (A–A′). The top diagram represents the raw data, the middle diagram is a bimodal Gaussian fit, and the bottom one is a unimodal Gaussian fit.

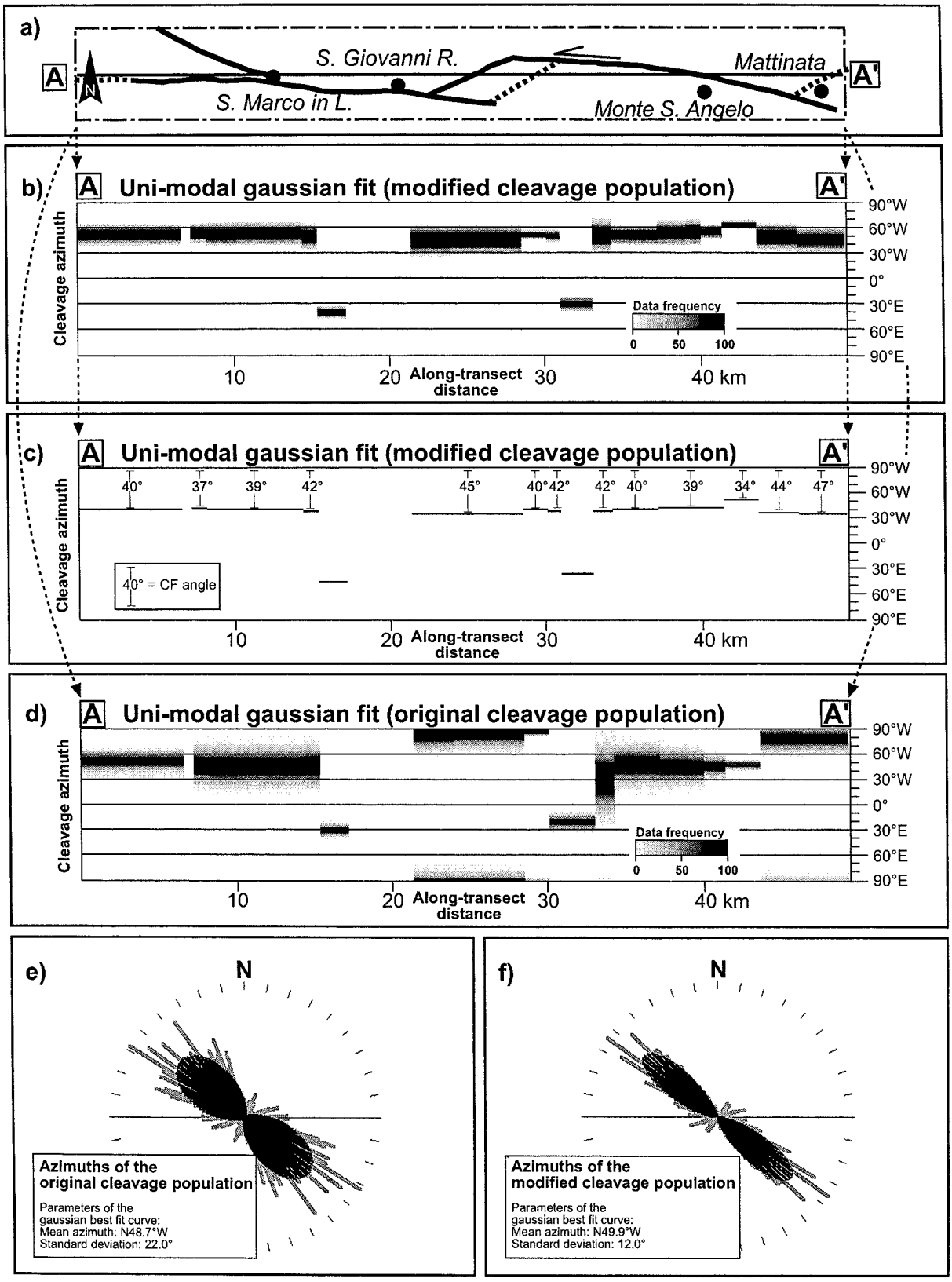

Fig. 8. Cleavage azimuths rotated to conform to an idealised Mattinata Fault having perfect E–W strike. (a) Trace of the Mattinata Fault and location (A–A′) of the structural transect swath. (b) Frequency of rotated cleavage azimuths with distance along the transect swath (A–A′). The local fault azimuth was determined for each sample location and the data azimuths were then rotated to conform to a fictitious E–W striking fault. (c) Lines representing the highest gaussian peaks from (b) showing the nearly constant mean trend of the rotated cleavage azimuths along the transect. (d) Original unrotated data repeating diagram from the bottom of Fig. 7(c). Note the decrease in scatter of (b) and (c) with respect to (d). (e) Rose diagram for the unrotated azimuthal cleavage data represented in (d). In grey is the histogram, in black is the curve resulting from the unimodal Gaussian fit. (f) Rose diagram for the rotated azimuthal data represented in (b). Histogram in grey, the curve resulting from the unimodal Gaussian fit is shown in black.

bounded by an interconnecting network of sheared solution surfaces and associated tip structures (Fig. 3e).

The sense of the shear displacement on the faults and on the associated sheared cleavage planes is synthetic. As a rule, the fault–cleavage intersection lines are normal to the strike-slip slickenlines (*sensu* Davis and Reynolds, 1996) on the fault surfaces as well as normal to the slickenside and/or slickolite lineations developed on the sheared solution cleavages, i.e. rotational axes (Wise and Vincent, 1965; Salvini and Vittori, 1982) of faults and of sheared solution surfaces are nearly parallel (Figs. 5 and 6).

Despite the observed shear displacement, the cleavage planes are never found to cross-cut or displace the related fault plane. The fault–cleavage intersection zone is normally a site of cataclastic, silt-sized carbonate grains forming a free boundary for fault slippage (Fig. 5b). Here, cleaved rocks show progressive comminutation into fault breccia or microbreccia. In approaching such a free boundary, the cleavage planes may be slightly convex in the direction of the relative fault slip (Fig. 5b).

4. Analysis of structural data

The total dataset from 42 sample sites within the Mattinata Fault Zone includes geometric and kinematic observations on a total of 2230 cleavage surfaces and 195 fault surfaces (Fig. 6).

Meso-scale faults within the Mattinata Fault Zone are strike-slip sub-vertical planes, which may be grouped into four main populations (Fig. 6): (1) E–W left lateral; (2) N55°W left-lateral; (3) N70°E left-lateral; and (4) N20°E right-lateral. Cleavages in the Mattinata Fault Zone are sub-vertical planes ranging in strike from nearly E–W to N10°W. A small cluster on the figure indicates a few cleavages striking N50°W with south dips.

Plotting cleavage data as separate rose diagrams (Fig. 7a) from the various segments of the Mattinata Fault (Fig. 7b) illustrates the heterogeneous pattern along strike of the fault. A more continuous spatial overview of details of changing cleavage azimuths along strike appears in the structural transect plots (Fig. 7c) in which cleavage azimuths are plotted by frequency versus the along-transect distance (see Appendix). Data plotted in these diagrams are cleavage azimuths from stations along the A–A′ transect swath of Fig. 7(b). The histogram diagram (above Fig. 7c) displays the frequency of the raw dataset, whereas in the bi- and unimodal Gaussian fit diagrams (lower in Fig. 7b) the dataset is filtered by bi- and unimodal Gaussian distributions, respectively, to show the main trends (see Appendix). In these diagrams, it is observed that the azimuths of the sampled cleavages tend to rotate clockwise or counter-clockwise from the overall N50°W trend (Fig. 6), respectively, in concert with the clockwise or counter-clockwise deviations of the fault trace from its average E–W orientation. The cleavage trend becomes nearly E–W along the N50°E fault segments in the two pull-apart basins and N20°W along the N60°W fault segments northwest of S. Marco in Lamis and west of Monte S. Angelo (Fig. 7a and c). On the other hand, where the fault trace is E–W oriented, cleavages tend to cluster along the N50°W direction. The comparison between the bi- and the unimodal Gaussian fits (Fig. 7c) shows that the two Gaussian curves identified in the bimodal distribution are close enough to fit into a unimodal Gaussian distribution.

5. The cleavage–fault angle

The cleavage–fault (CF) angle is here defined as the dihedral angle between the cleavage and the fault plane (Fig. 5). As seen in the previous section, the variations in azimuth of the Mattinata Fault seem to correspond to equivalent variations in strike of the associated cleavage surfaces. Therefore, a rather constant CF angle can be seen to occur along the entire length of the fault. As a test of this hypothesis, variations in the CF angle were statistically assessed along a specific structural transect. In that both the Mattinata Fault and its associated cleavages are sub-vertical, the cleavage–fault angle can be designated as their difference in azimuth. To plot local measurements of the CF angle, the local strike of the fault at each station was determined from our field data and/or from maps after previous papers (Funiciello et al., 1988 and references therein). The cleavage azimuthal data for each local station were then rotated to correspond to a theoretical E–W fault strike. In this way, the relative constancy of the CF angle can be seen as straight lines in Fig. 8(b) and (c).

The modified cleavage azimuth dataset was georeferenced like the original one and then plotted using the same A–A′ transect swath of Fig. 7(b). From the comparison between the original cleavage azimuth domain (Fig. 8d and e) and the modified one (Fig. 8b and f), the dependence of the cleavage pattern upon the fault orientation can be inferred. The scattering of the azimuth population in terms of standard deviation is reduced by 10°, from 22° to 12°, around a mean azimuth of about N50°W (Fig. 8e and f). The nearly constant line of Gaussian peaks at about N50°W (Fig. 8c) reflects the constancy of the CF angle through the changes in azimuth of the Mattinata Fault (Fig. 8a). The CF angle slightly increases in the two pull-aparts, whereas the minimum value is reached in the transpressional fault segment near Monte S. Angelo.

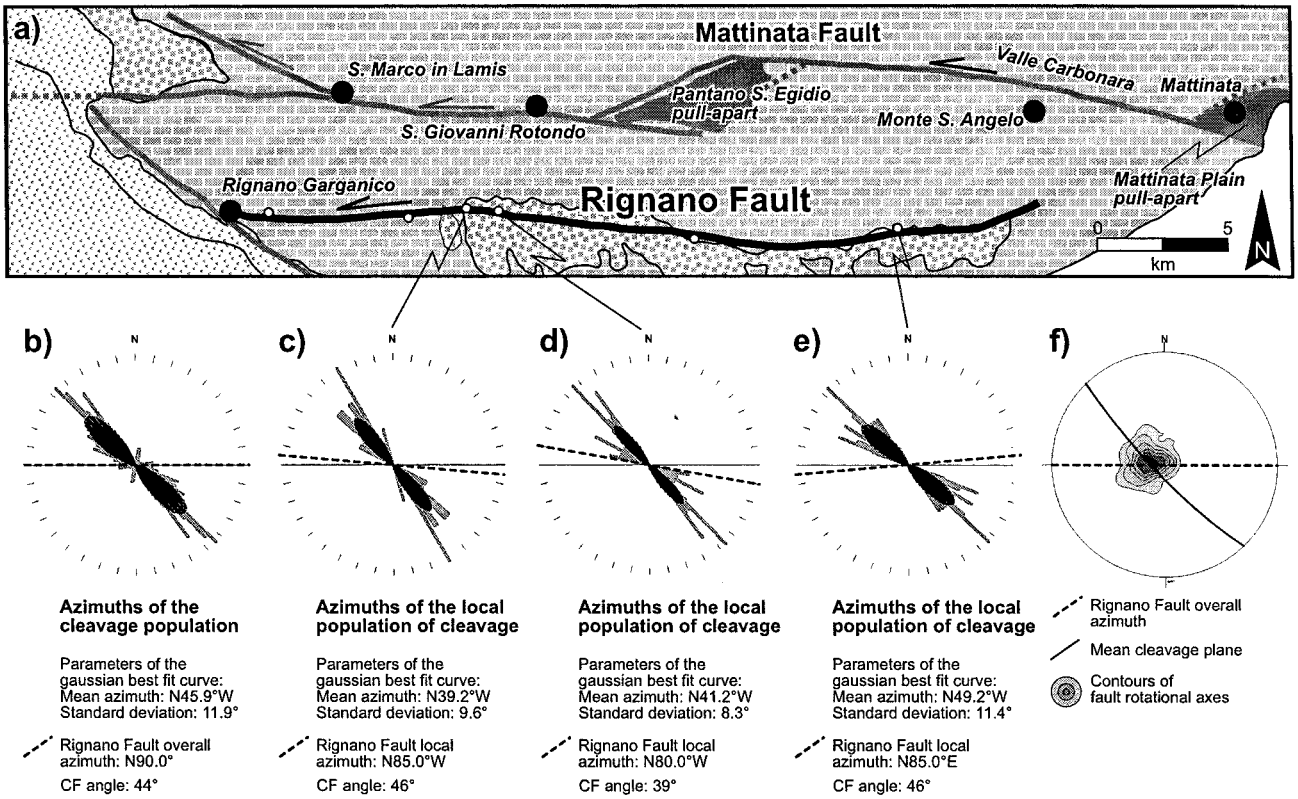

Fig. 9. (a) Geological map of the area surrounding the Rignano Fault. For the Legend see Fig. 1. (b) Cumulative rose diagrams for the entire set of cleavage azimuths sampled along the fault. (c), (d) and (e) Rose diagrams showing cleavage azimuths from specific segments of the Rignano Fault indicated by the connecting lines. In grey is the histogram, in black is the curve resulting from the unimodal Gaussian fit. Each diagram also shows the local azimuth of the Rignano Fault as a dashed line to illustrate the relative constancy of the cleavage–fault angle at each site. (f) Contoured stereogram (Schmidt projections, lower hemisphere) with a single maximum showing the overall parallelism among fault rotational axes (data no. = 45) and the fault–cleavage intersection line.

The rose-diagram of Fig. 8(f) represents the cumulative histogram and unimodal Gaussian fit of the modified cleavage population. The mean CF angle of about 40°, with a standard deviation of 12°, can be read as the distance from the mean azimuth value of the Gaussian curve (i.e. N50°W) to the E–W direction. The mean 40° CF angle value accounts for the normal scattering of the CF angle (i.e. related to fault anastomosing, fault branching, and local rheological variations) as well as the opposite variations of the CF angle in the transtensional and the transpressional fault segments.

6. Comparison with the Rignano Fault

The E–W Rignano Fault is located in the same carbonate formations about 4 km south of the Mattinata Fault (Fig. 9a) with an on-shore length of about 40 km. The most obvious deformation features along it are sub-vertical minor strike-slip faults and cleavage surfaces analogous to those along the Mattinata Fault. Within the Rignano Fault Zone, horizontal slickenlines along the fault surfaces and NW–SE solution cleavages indicate its left-lateral strike-slip kinematics. However, about 400 m of vertical topographic offset along this fault as well as vertical slickenlines overprinting horizontal ones suggest a younger vertically moving reactivation. Exposures along the fault show a mean azimuth of cleavage at about N46°W with a standard deviation of about 12° (Fig. 9b). Assuming an overall E–W trend of the fault, the resulting average CF angle is equal to 44° (Fig. 9b). Assessments of the CF angle in three major exposures along the fault yield values of 46°, 39° and 46° (plots of Fig. 9c, d and e) based on the difference between the local fault azimuth and the best Gaussian fit of cleavage azimuths at each station (Fig. 9a).

The polar diagram of Fig. 9(f) shows the contours of the fault rotational axes together with the projection of the overall E–W vertical fault plane and the average plane of cleavage (i.e. N46°W-striking, 85°NE-dipping). Plotted fault rotational axes are only those associated with the strike-slip indicators. The plot

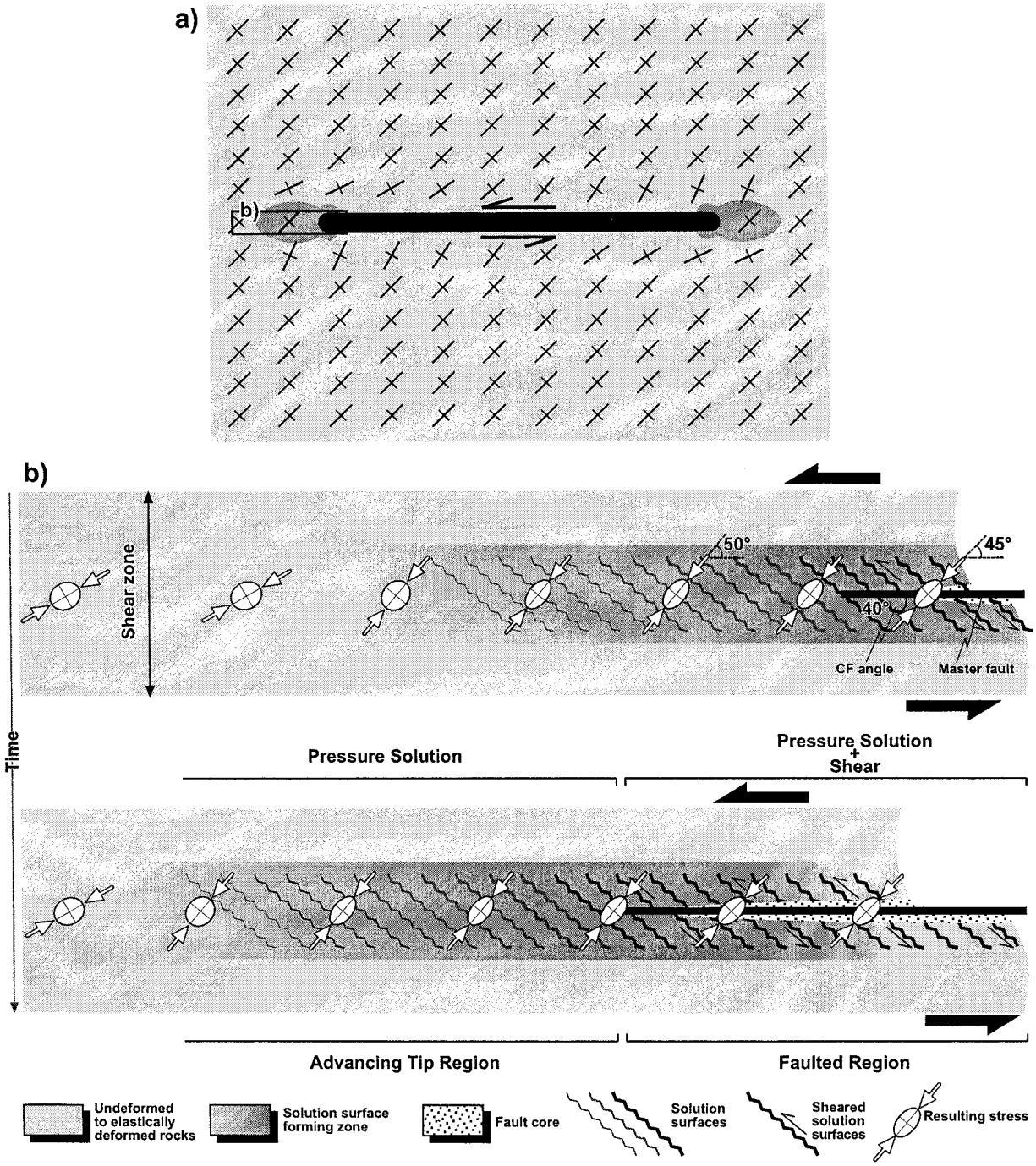

Fig. 10. Model for the cleavage nucleation and growth. (a) Stress trajectories for a mode II crack loaded by pure remote shear (modified after Pollard and Segall, 1987). Longer tics are parallel to the maximum compression stress and shorter tics are parallel to the maximum tensile stress. Lengths of tics do not indicate stress magnitude. Stresses are normal or parallel to the crack walls that are shear strength free. Shading at the crack tips schematically indicates the regions of stress concentration in the prolongations of the fault (after Chinnery, 1961, 1963 and Pollard and Segall, 1987). The scale is not indicated because the model is scale-invariant. In this case, the mode II crack of the figure represents an analogue of the Mattinata Fault whose associated zone of deformation is approximately 200 m wide. (b) With fault propagation, the enhanced stress at the fault tip nucleates solution cleavages in the distal part of the region of stress concentration. As the fault advances some of the nascent cleavage planes are reactivated in a dominantly shear mode that includes some slickolite redeposition. Finally, the master fault cuts through all the tip zone structures producing gouge, breccia and local minor drag of the truncated cleavages.

demonstrates the overall parallelism among the subvertical lines of fault-cleavage intersection, fault rotational axes and rotation axes from the sheared solution surfaces.

7. Model for development of the fault-related cleavage

Key geometric and kinematic features of the Mattinata Fault Zone are: (a) a set of parallel, adjoining surfaces form two types of fault-related cleavage, simple solution surfaces and shear reactivated surfaces; (b) the cleavage is restricted to 200–300-m-wide fault zones; (c) the intersection lines between the fault and associated cleavage surfaces are parallel to the rotation axes derived from motion indicators on both the fault and the sheared solution surfaces; (d) sense of motion indicators are synthetic for both faults and sheared solution surfaces; and (e) even though the fault azimuth may change locally, the cleavage–fault angle remains relatively constant at about 40°.

These features can be synthesised into the following model for the cleavage development (Fig. 10). Cleavage surfaces form during the fault propagation by pressure solution within carbonate rocks strained by the stress concentration in the region ahead of the advancing fault tip. Rock strength and relative motion of fault blocks produce a local stress regime (i.e. kinematic stress) within this region (Fig. 10b). For relative movements parallel to the fault plane, maximum and minimum stress axes lie at 45° from the fault plane (e.g. Sanderson and Marchini, 1984). With these conditions, the pressure solution planes would develop at an angle of 45° to the fault plane. The average 40° cleavage–fault angle found along the Mattinata Fault suggests a slight rotation of the maximum axis of the local stress away from the fault plane. McKinnon and Garrido de la Barra (1998), in numerical experiments reproducing simple shear-related fracturing and stress fields, achieved analogous results in which a progressive rotation away from the applied shear of the major principal stress arose before fracturing took place.

This model, together with the observations on the spatial distribution of cleavage and its displacements can be integrated into a fault propagation cleavage model for temporal evolution of the Mattinata Fault (Fig. 10). Fault propagation started with the formation of an array of solution surfaces oriented at 40° from the fault plane in front of its tip region, where stress concentration occurs (Chinnery, 1963). The shear displacements, synthetic with the fault motion (i.e. left lateral), of the re-activated cleavage planes suggest that the rotation of the stress away from the fault involved only the cleavage development regime in the near-tip region. As the fault zone propagated, the former tip region was integrated into the fault zone and the solution cleavages were cut and offset by the advancing array of slip planes. With continued slip in the fault zone, where the kinematic stress recovers to its theoretical orientation (i.e. with the maximum axis at 45° from the fault plane), part of the cleavage surfaces was reactivated according to synthetic strike-slip motions. Once formed, the solution cleavages became significant planes of anisotropy ready to be reactivated during subsequent fault growth. Commonly, dilation wing fractures emanated from the tips of the sheared cleavage planes to interconnect into a fracture network. For the most part, the shear deformation along the cleavage planes was slow enough to allow some calcite solution and redeposition as slickolite fibres. Eventually, with continued slip, the fault core produced gouge and cataclasite as overprints on the slightly older, cleaved damage zone. Minor, local fault drag of the cleavage planes just beside the slip surface occurred in this phase, resulting in a slight decrease in the cleavage–fault (CF) angle near the fault plane. This model is analogous to that of Petit and Barquins (1988) in which, properly oriented, échelon, mode I fractures rather than solution cleavages, are the precursory structures propagating ahead of the fault tip.

In the absence of appropriate key outcrops, direct observation of tip structures was not possible. Nevertheless, three principal features justify the interpretation of the Mattinata Fault cleavage as fault-propagation structures: (1) rock faulting is always anticipated by some degree of stress/strain concentration in front of the growing fault (Chinnery, 1961, 1963; Pollard and Segall, 1987); (2) fault strength weakening (Mandl, 1988) is likely to prevent the development of new cleavage surfaces in the fault damage zone once the fault core has developed; (3) no cleavages were found to be associated with the dip-slip reactivation of the Rignano Fault.

Several authors (Willemse and Pollard, 1998 and references therein) have discussed wing fractures and solution seams emanating from the termination of small shear fractures (e.g. deformations associated with the small faults exposed in carbonates from the Languedoc region, France; Rispoli, 1981). They observed that veins and pressure solution surfaces emanate from near the ends of small, left lateral faults and hypothesised that the tensile/compressive stress concentrations at the fault tip sides, resulting from slip on the faults, caused the veins and solution surfaces to form and propagate away from these structures. Pollard and Segall (1987) numerically demonstrated that these features have a theoretical kink angle (*sensu* Willemse and Pollard, 1998) of 70.5° from the fault plane. Willemse and Pollard (1998) presented analytical solutions for the case of a zone of high strength or friction at a shear crack termination (Ida, 1972; Palmer and Rice, 1973; Cowie and Scholz, 1992). They

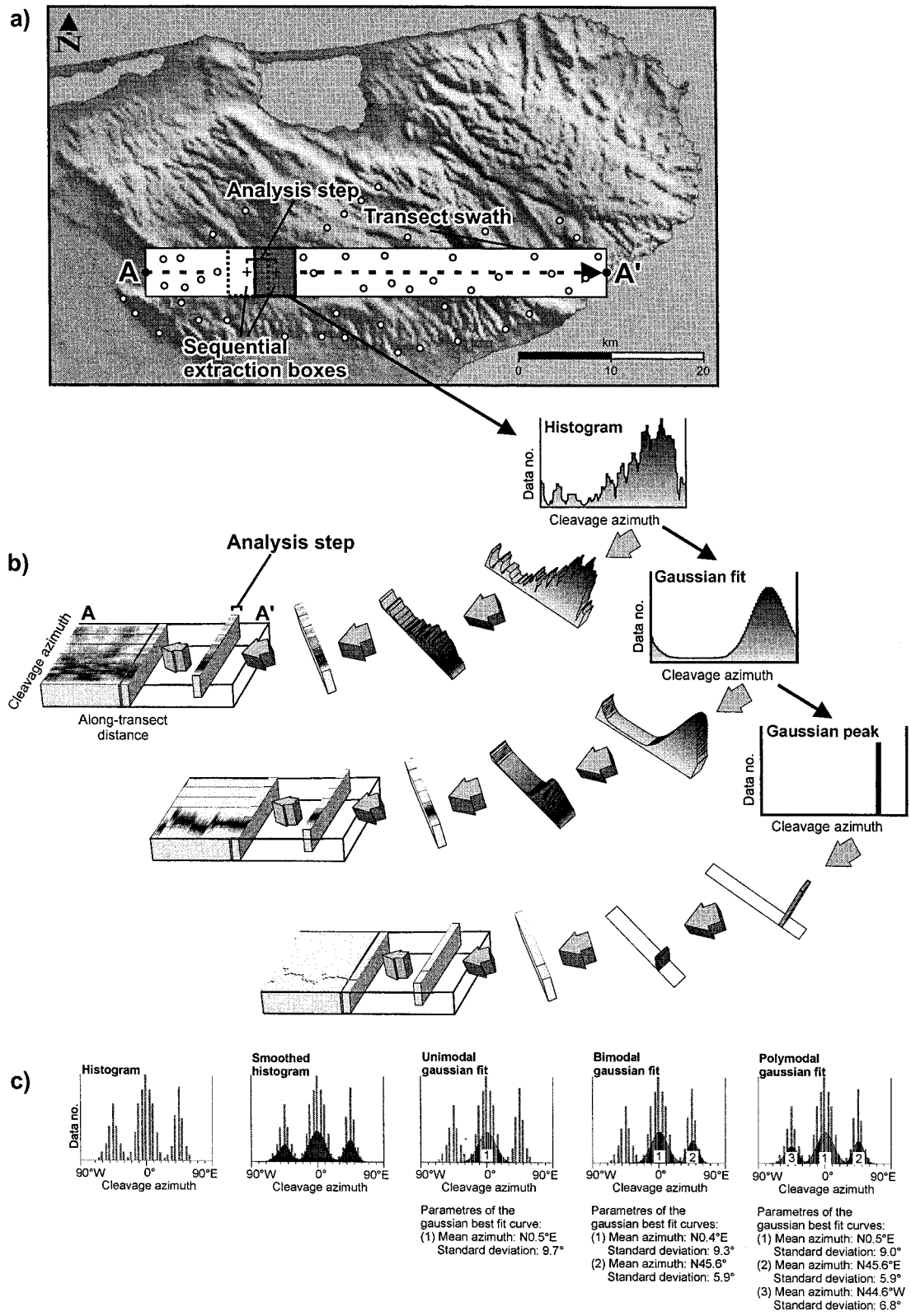

Fig. 11. Structural transect methodology applied to (fictitious) cleavage azimuth data along the Mattinata Fault. (a) Example of a transect swath including the Mattinata Fault zone in the Gargano area. The white rectangular box is the area of the A–A′ transect swath. The white-filled dots represent (fictitious) sample stations in the Gargano area. Two boxes within the transect swath are examples of sequential analysis boxes. Data contained in each of these boxes are those extracted to form the raw dataset of each single histogram in (b). The analysis box is advanced by the analyis step. The analytical process is then repeated at each step to complete the A–A′ transect swath. Some overlap of the extraction boxes is used to smooth the data along the structural transect plots. (b) Construction of the structural transects by adding in sequence, along the length of the transect, the single histograms (or Gaussian fits/peaks). Each histogram refers to a single extraction box and occupies along the transect plot, a width equal to the analysis step along the transect swath. (c) Stages in azimuth–frequency Gaussian fitting analysis. From left to right: raw data histogram; raw data histogram (grey) and smoothed histogram (black); raw data histogram (grey) and unimodal Gaussian fit curve (black); raw data histogram (grey) and bimodal Gaussian fit curves (black); raw data histogram (grey) and polymodal Gaussian fit curves (black).

showed that instead of emanating from the tip sides, the tip structures can develop straight through the crack plane slightly ahead of the tips, with drastic reduction in the theoretical kink angle. In addition to the size of the structures, at least two important issues distinguish the solution cleavage within the Mattinata Fault Zone from that of fault-related wing surfaces. (1) Solution (wing) seams associated with small faults are spatially distributed as isolated or discrete small arrays of surfaces along the fault plane, typically at the fault tips. Cleavage within the Mattinata Fault Zone is made of closely spaced planes continuous throughout the entire fault length. (2) Solution seams associated with small faults are restricted to the two near-tip contractional quadrants and are hypothesised to develop mostly by the local increase in the mean normal component of the stress field (Pollard and Segall, 1987). Cleavage within the Mattinata Fault develops by the stress concentration in the prolongation of the advancing fault.

8. Conclusions

1. Solution cleavages that characterise the Mattinata Fault Zone developed in carbonate rocks of the Gargano Promontory. The cleavage is confined within the about 200-m-wide fault zone.
2. Within the framework of the Mattinata Fault Zone, cleavage formation can be related to rock dissolution processes associated with the stress concentration ahead of the advancing tip. As the cleavage system developed in the propagating fault zone, further growth of several cleavage surfaces occurred by both pressure solution and enhancement by shear mechanisms.
3. Within the Mattinata Fault Zone, solution cleavage developed according to geometrical rules relating cleavage spacing and the cleavage–fault angle to fault slip and fault sense of motion.
4. The average cleavage–fault angle of 40° along the Mattinata Fault also seems to apply to the Rignano Fault. This angle may be useful in determining geometry and kinematics of poorly exposed faults.
5. The mechanisms of cleavage development and reactivation along propagating fault zones of the Gargano area bear significant implications for secondary permeability in hydrocarbon and other fluid reservoirs. Closely spaced solution cleavages, although originally generated as tight solution seams, may be opened by fluid overpressure as disjunctive cleavages to increase rock permeability in selected directions within fault zones, as observed in the well cores from oil producing carbonates in the Southern Apennines. The dilation fractures developed at the tip of the sheared solution surfaces improve the fracture network connectivity. Mapping of variations in orientation of the studied cleavage may provide indications for the potential migration paths for fluids as well as locate zones of increased permeability along a major fault system network.

Acknowledgements

Thanks are due to R. Funiciello for encouraging our work and to F. Storti for useful discussions. Digital elevation data of Fig. 11(a) is courtesy of N. D'Agostino, Roma Tre University. A. Billi is grateful to A. Aydin for helpful advice on fracture mechanics during a field trip to Southern Apennines. Financial support was from Italian MURST (grants 60% to F. Salvini). A. Billi's work was partly funded by the Commission of European Communities (Contract No. ENV4-CT96-0291) through the Istituto Nazionale di Geofisica of Rome. The paper greatly benefited from reviews by D. Peacock and an anonymous reviewer, and from suggestions by the associate editor T. Blenkinsop.

Appendix

A.1. Structural transect plot methodology

In this Appendix we illustrate the methodology and procedures for the construction of the structural transect plots, which were used in this paper to derive the spatial organisation of the cleavage surfaces along the Mattinta Fault (Figs. 7 and 8).

The term structural transect describes a three-dimensional plot (Fig. 7c) in which a property (i.e. a variable) characterising a particular geological entity over the study area (e.g. the strike, dip, spacing, aperture or length of structural surfaces) is graphed by its frequency along the transect distance. The analysed measurements of the variable are those falling within a selected map transect swath whose distance represents the plot abscissa (i.e. the along-transect distance; Fig. 11a).

The structural transect method combines the azimuth-versus-transect-distance (AVTD) philosophy (Wise and McCrory, 1982) with data filtering and statistical analysis by uni- to polymodal Gaussian fitting automated techniques (Funiciello et al., 1977; Wise et al., 1985; Salvini, 1991a, b). Namely, structural measurements from scattered stations are integrated within a transect swath into running averages of the

variable along the selected map transect swath. The advantages of employing the structural transect technique with spatially referenced structural data is twofold: (1) the merging of scattered data into a spatially continuous diagram aids the detection and evaluation of their spatial relationships; and (2) structural patterns at non-sampled locations can be partially predicted from sampled locations. In addition, the application of the Gaussian best fit to the raw data allows the statistical characterisation of the main trends in the sampled populations and the identification of mean and standard deviation values. The entire process is integrated into the DAISY 2.1 package (Structural Data Integrated System Analyser; Salvini, 1998).

The procedure is illustrated in the sketch of Fig. 11(a), where fictitious measurement stations in the Gargano area are represented by white-filled dots. The structural transect relative to the A–A′ transect swath is prepared using selected, referenced data from the scattered measure stations falling within the transect swath (Fig. 11a). Width and length of the swath are chosen according to the purpose of the analysis.

The procedure steps may be summarised as follows.

1. Data gathered in the stations is filed in the software database with geographical references, e.g. latitude and longitude of cleavage azimuth measurement stations in the example of Fig. 11.
2. An appropriate transect swath axis is chosen across the map (the segment A–A′ in Fig. 11a) and the proper half-width across the segment is chosen to derive the extraction swath; that is the area from which data are selected for the analysis. In the example (Fig. 11a), this width is 2500 m, for we intend to analyse the azimuth pattern of cleavage within a swath 5000 m wide.
3. A set of frequency analyses are performed in spatial sequence along the A–A′ segment. An analysis step is selected, depending upon the needed spatial resolution of the analysis along the transect (Fig. 11a). At each step, data falling within a rectangular area (extraction box in Fig. 11a), which has one side coinciding with the transect swath width and the other arbitrarily chosen, are processed and the relative frequency histograms carried out (Fig. 11b). The box and the analysis step lengths are properly chosen in order to guarantee some overlap between the datasets of adjacent analyses, i.e. the box length is normally greater than the analysis step (Fig. 11a).

   The overlap between adjacent analyses produces an along-swath running average which allows one both to fill gaps produced by the station scattering and to enhance the continuity (and therefore the visibility) of spatial, along-swath trends (Fig. 11b). This implies that data from each measurement station are usually extracted for more than one analysis, depending upon the overlap between adjacent analyses (Fig. 11a).

   The statistical processing can be handled by a series of options according to the purpose of the analysis. Histograms can be smoothed to reduce noise component of the raw data (Fig. 11c). The smoothing procedure consists of a selected number of moving weighted averages which reduce noise in discontinuous data (Davis, 1973; Funiciello et al., 1977; Wise and McCrory, 1982; Wise et al., 1985; Salvini, 1991b). At each i interval, the smoothed value Y_i' is computed by:

$$Y_i' = \frac{\sum_{j=i-k/2}^{i+k/2} Y_j}{k} \tag{A1}$$

   where k is the width of the smoothing interval.

   The appropriate number and values of weighted smoothing is chosen by the analyst on the basis of the data density and on the purpose of the structural analysis (i.e. regional versus local trend enhancement).

   The frequency of each histogram may be usefully normalised within the 0–100 range to allow the comparison among frequency analysis with differing numbers of data.
4. Each histogram is then fitted to one or more Gaussian curves through a best-fit algorithm (Salvini, 1991a, 1998), in order to detect and characterise each meaningful trend within the dataset (Fig. 11b and c). The fitting Gaussian distribution centered around the preferential smoothed values is of the type (Fraser and Suzuki, 1966)

$$f(x) = \sum_{i=1}^{N} h_i \exp\left[-4\, ln\, 2 \left(\frac{x - m_i}{\Delta_i} \right) \right]^2 \tag{A2}$$

   where x is the variable (cleavage azimuths in this paper), h is the peak height, m is the mean value of x, N the number of significant distributions and:

$$\Delta_i \cong \sigma_i \sqrt{2_i} \tag{A3}$$

   where σ_i is the standard deviation of the i Gaussian.

   The given dataset to be fitted by the Gaussian distribution may be dealt with by the analyst as unimodal or polymodal. When the unimodal Gaussian fit is progressed, the best fitting Gaussian curve within the smoothed dataset will be identified (Fig. 11c). The curve will fit the entire dataset or a portion of it depending upon its real distribution. On the other hand, polymodal Gaussian fits to unimodally-distributed datasets will always identify only a single, major Gaussian curve. This process is

partly controlled by the analyst who decides the minimum value of relative height for a peak to be meaningful and the shape of the initial fitting Gaussian curve (Eq. A2). Progressing the bimodal or polymodal fit will allow for identification of the two or more best fitting Gaussian curves within the smoothed dataset (Fig. 11c).

5. Histograms or Gaussian fits are used to prepare the final output, the structural transects (Fig. 11b). Each histogram or Gaussian fit relative to a single (box) analysis is projected on a diagram where the x-axis represents the distance along the A–A′ segment and the y-axis is the range of values of the analysed variable (Fig. 11b). The frequency of the variable, plotted along the z-axis, either as histogram or as Gaussian fit, is graphed through shading (Fig. 11b). The peak value of the Gaussian fitting curves can be isolated and plotted versus the transect length as a series of points to yield a line of data points showing variations in the average azimuth of that particular peak feature along the line of transect (Fig. 11b).
6. Usual histogram (Fig. 11c) or a rose plot may also individually represent results from each histogram. In these cases, the plot of single Gaussians as independent curves in the same plot results in a particularly efficient way to visualise the found trends. In this paper, specific rose diagrams relative to frequency of cleavage azimuths have been coupled to the structural transects (Figs. 7 and 8), in order to ease their first examination.

The transect preparation software is included in the structural data analyser software DAISY 2.1 (Salvini, 1998). This package is available as freeware to scientific institutions and academics via e-mail (salvini@uniroma3.it).

References

Alvarez, W., Engelder, T., Lowrie, W., 1976. Formation of spaced cleavage and folds in brittle limestone by dissolution. Geology 4, 698–701.

Andrews, L.A., Railsback, L.B., 1997. Controls on stylolite development: morphologic, lithologic and temporal evidence from bedding-parallel and transverse stylolites from the U.S. Appalachians. Journal of Geology 105, 59–73.

Arthaud, F., Mattauer, M., 1969. Exemples de stylolites d'origine tectonique dans le Languedoc, leurs relations avec la tectonique cassante. Bulletin de la Societé Géologique de France 11, 738–744.

Ashby, M.F., Hallam, S.D., 1986. The failure of brittle solids containing small cracks under compressive stress states. Acta Metallurgica 34, 497–510.

Aydin, A., Schultz, R.A., 1990. Effect of mechanical interaction on the development of strike-slip faults with en-échelon patterns. Journal of Structural Geology 12, 123–129.

Aydin, A., 1988. Discontinuities along thrust faults and the cleavage duplexes. In: Mitra, G., Woytal, S. (Eds.), Geometries and Mechanics of Thrusting. Geological Society of America, Special Publication 222, pp. 223–232.

Bell, T.H., 1978. The development of slaty cleavage across the Nackara Arc of the Adelaide geosyncline. Tectonophysics 51, 171–201.

Berthé, D., Chokroune, P., Jegouzo, P., 1979. Orthogneiss, mylonite and noncoaxial deformation of granites: the example of the South Armorican shear zone. Journal of Structural Geology 1, 127–133.

Biju-Duval, B., Dercourt, J., Le Pichon, X., 1977. From the Tethys Ocean to the Mediterranean Seas: a plate tectonic model of the evolution of the western Alpine system. In: Biji-Duval, B., Montadert, L. (Eds.), The Structural History of the Mediterranean Basins. Technip, Paris, pp. 143–167.

Bosellini, A., Neri, C., Luciani, V., 1993. Platform margin collapses and sequence stratigraphic organization of carbonate slopes: Cretaceous–Eocene, Gargano Promontory, Southern Italy. Terra Nova 5, 282–297.

Brace, W.F., Bambolakis, E.G., 1963. A note on brittle crack growth in compression. Journal of Geophysical Research 68, 3709–3713.

Brace, W.F., Paulding, B.W., Scholz, C.H., 1966. Dilatancy in the fracture of crystalline rocks. Journal of Geophysical Research 71, 3939–3942.

Caine, J.S., Evans, J.P., Forster, C.B., 1996. Fault zone architecture and permeability structure. Geology 24, 1025–1028.

Carannante, G., Guzzetta, G., 1972. Stiloliti e sliccoliti come meccanismo di deformazione delle masse rocciose. Bollettino della Società dei Naturalisti in Napoli 81, 157–170.

Chernyshev, S.N., Deanman, W.R., 1991. Rock Fractures. Butterworth-Heinemann, London.

Chinnery, M.A., 1961. The deformation of the ground around surface faults. Bulletin of the Seismological Society of America 51, 355–372.

Chinnery, M.A., 1963. The stress changes that accompany strike-slip faulting. Bulletin of the Seismological Society of America 53, 921–932.

Choukroune, P., 1969. Un exemple d'analyse microtectonique d'une série calcaire affectée de plis isopaques. Tectonophysics 7, 57–70.

Cooke, M.L., Pollard, D.D., 1996. Fracture propagation paths under mixed mode loading within rectangular blocks of polymethyl methacrylate. Journal of Geophysical Research 101, 3387–3400.

Cooke, M.L., 1997. Fracture localization along faults with spatially varying friction. Journal of Geophysical Research 102, 22425–22434.

Cotterell, B., Rice, J.R., 1980. Slightly curved or kinked cracks. International Journal of Fracture 16, 155–169.

Cowie, P.A., Scholz, C.H., 1992. Physical explanation for the displacement–length relationship of faults, using a post-yield fracture mechanics model. Journal of Structural Geology 14, 1133–1148.

Cox, S.J.D., Scholz, C.H., 1988. Rupture initiation in shear fracture of rocks: an experimental study. Journal of Geophysical Research 93, 3307–3320.

Cruikshank, K.M., Zhao, G., Johnson, A.M., 1991. Analysis of minor fractures associated with joints and faulted joints. Journal of Structural Geology 13, 865–886.

Davis, G.H., Reynolds, S.J., 1996. Structural Geology of Rocks and Regions. John Wiley, New York.

Davis, J.C., 1973. Statistics and Data Analysis in Geology. John Wiley, New York.

Dieterich, J.H., 1969. Origin of cleavage in folded rocks. American Journal of Science 267, 155–165.

Dunnington, H.V., 1954. Stylolite development post-dates rock induration. Journal of Sedimentary Petrology 24, 27–49.

Engelder, T., Geiser, P., 1979. The relationship between pencil clea-

vage and lateral shortening within the Devonian section of the Appalachian Plateau, New York. Geology 7, 460–464.
Erdogan, F., Sih, G.C., 1963. On the crack extension in plates under plane loading and transverse shear. Journal of Basic Engineering 85, 519–527.
Favali, P., Funiciello, R., Salvini, F., 1993b. Geological and seismological evidence of strike-slip displacement along the E–W Adriatic–Central Apennine belt. In: Boschi, E. (Ed.), Recent Evolution and Seismicity of the Mediterranean Region. Publication of the Istituto Nazionale di Geofisica, Rome, pp. 333–346.
Favali, P., Funiciello, R., Mattietti, G., Mele, G., Salvini, F., 1993a. An active margin across the Adriatic Sea (central Mediterranean Sea). Tectonophysics 219, 109–117.
Fraser, R.D.B., Suzuki, E., 1966. Resolution of overlapping absorption bands by least squares procedures. Analytical Chemistry 38, 1770–1773.
Funiciello, R., Parotto, M., Salvini, F., Locardi, E., Wise, D.U., 1977. Correlazioni tra lineazioni rilevate con il metodo "Shadow" e assetto tettonico nell'area vulcanica del Lazio. Bollettino di Geodesia e Scienze Affini 4, 451–470.
Funiciello, R., Montone, P., Salvini, F., Tozzi, M., 1988. Caratteri strutturali del Promontorio del Gargano. Memorie della Società Geologica Italiana 41, 1235–1243.
Funiciello, R., Montone, P., Parotto, M., Salvini, F., Tozzi, M., 1991. Geodynamical evolution of an intra-orogenic foreland: the Apulia case history (Italy). Bollettino della Società Geologica Italiana 110, 419–425.
Gaviglio, P., 1986. Crack–seal mechanisms in limestone: a factor of deformation in strike-slip faulting. Tectonophysics 131, 247–253.
Gratier, J.P., Gamond, J.F., 1990. Transition between seismic and aseismic deformation in the upper crust. In: Knipe, R.J., Rutter, E.H. (Eds.), Deformation Mechanisms, Rheology and Tectonics. Geological Society, London, Special Publication 54, pp. 461–473.
Griffith, A.A., 1924. Theory of rupture. In: Biezeno, C.B., Burgers, J.M., Waltman, J. (Eds.), Proceedings of the First International Congress on Applied Mechanics, Delft, pp. 55–63.
Groshong Jr., R.H., 1975. "Slip" cleavage caused by pressure solution in a buckle fold. Geology 3, 411–413.
Groshong Jr., R.H., 1988. Low-temperature deformation mechanisms and their interpretation. Geological Society of America Bulletin 100, 1329–1360.
Guerricchio, A., 1986. Esempi di bacini di pull-apart nel Gargano (Puglia settentrionale). Geologia Applicata e Idrogeologia 21, 25–36.
Guzzetta, G., 1984. Kinematics of stylolite formation and physics of the pressure-solution process. Tectonophysics 101, 383–394.
Henderson, J.R., Wright, T.O., Henderson, M.N., 1986. A history of cleavage and folding: an example from the Goldenville Formation, Nova Scotia. Geological Society of America Bulletin 97, 1354–1366.
Hoek, E., Beniawski, Z.T., 1965. Brittle fracture propagation in rock under compression. International Journal of Fracture 1, 137.
Homberg, C., Hu, J.C., Angelier, J., Bergerat, F., Lacombe, O., 1997. Characterization of stress perturbations near major fault zones: insights from 2-D modelling and field studies (Jura Mountains). Journal of Structural Geology 19, 703–718.
Horii, H., Nemat-Nasser, S., 1985. Compression-induced microcrack growth in brittle solids: axial splitting and shear failure. Journal of Geophysical Research 90, 3105–3125.
Horii, H., Nemat-Nasser, S., 1986. Brittle failure in compression: splitting, faulting and brittle–ductile transition. Philosophical Transactions of the Royal Society of London A319, 337–374.
Hsü, K.J., 1982. Alpine–Mediterranean geodynamics: past, present and future. In: Berckhemer, H., Hsü, K.J. (Eds.), Alpine–Mediterranean Geodynamics. American Geophysical Union–Geological Society of America, Geodynamic Series 7, pp. 7–14.
Hyett, A.J., 1990. Deformation around a thrust tip in Carboniferous limestone at Tutt Head, near Swansea, South Wales. Journal of Structural Geology 12, 47–58.
Ida, Y., 1972. Cohesive force across the tip of longitudinal shear crack and Griffith specific surface energy. Journal of Geophysical Research 77, 3796–3805.
Illies, H., Greinier, G., 1978. Rhinegraben and the Alpine system. Geological Society of America Bulletin 89, 770–782.
Illies, H., Greinier, G., 1979. Holocene movements and the state of stress in the Rhinegraben rift system. Tectonophysics 52, 349–359.
Illies, H., 1975. Intraplate tectonics in stable Europe as related to plate tectonics in the Alpine system. Geologische Rundschau 64, 677–699.
Irwin, G.R., 1957. Analyses of stresses and strains near the end of a crack traversing a plate. Journal of Applied Mechanics 24, 361–364.
Kelly, P.G., Sanderson, D.J., Peacock, D.C.P., 1998. Linkage and evolution of conjugate strike-slip fault zones in limestones of Somerset and Northumbria. Journal of Structural Geology 20, 1477–1493.
King, G.C.P., Stein, R.S., Lin, J., 1994. Static stress changes and the triggering of Earthquakes. Bulletin of the Seismological Society of America 84, 935–953.
Lyakhovsky, V., Yehuda, B.Z., Amotz, A., 1997. Distributed damage, faulting, and friction. Journal of Geophysical Research 102, 27635–27649.
Mandl, G., 1988. Mechanics of Tectonic Faulting. Elsevier, Amsterdam.
Manzoni, M., Vandenberg, J., 1982. Perityrrhenian paleomagnetic data and the setting of the Calabria arc. In: Mantovani, E., Sartori, R. (Eds.), Structure, Evolution and Present Dynamics of the Calabrian Arc, Earth Evolutive Science 3, pp. 181–186.
Marshak, S., Engelder, T., 1985. Development of cleavage in limestones of a fold–thrust belt in Eastern New York. Journal of Structural Geology 7, 345–359.
Martel, S.J., 1997. Effects of cohesive zones on small faults and implications for secondary fracturing and fault trace geometry. Journal of Structural Geology 19, 735–747.
McGrath, A.G., Davison, I., 1995. Damage zone geometry around fault tips. Journal of Structrual Geology 17, 1011–1024.
McKinnon, S.D., Garrido de la Barra, I., 1998. Fracture initiation, growth and effect on stress field: a numerical investigation. Journal of Structural Geology 20, 1673–1689.
Mitra, G., Yonkee, W.A., 1985. Relationship of spaced cleavage to folds and thrusts in the Idaho–Utah–Wyoming thrust belt. Journal of Structural Geology 7, 361–373.
Mitra, G., Yonkee, W.A., Gentry, D.J., 1984. Solution cleavage and its relationship to major structures in the Idaho–Utah–Wyoming thrust belt. Geology 12, 354–358.
Nemat-Nasser, S., Horii, H., 1982. Compression-induced nonplanar crack extension with application to splitting, exfoliation and rockburst. Journal of Geophysical Research 87, 6805–6821.
Nickelsen, R.P., 1972. Attributes of rock cleavage in some mudstones and limestones of the Valley and Ridge province, Pennsylvania. Pennsylvania Academy of Science 46, 107–112.
Nickelsen, R.P., 1986. Cleavage duplexes in the Marcellus Shale of the Appalachian foreland. Journal of Structural Geology 8, 361–371.
Odom, A.L., Dunn, D.E., Engelder, J.T., Geiser, P.A., Kish, S.A., Hatcher, R.D., Schamel, S., Wise, D.U., 1980. A characterization of faults in the Appalachian foldbelt. Nuclear Regulatory Commission, Publication NUREG/CR-1621, Washington, DC.
Ohlmacher, G.C., Aydin, A., 1995. Progressive deformation and fracture patterns during foreland thrusting in the southern Appalachians. American Journal of Science 295, 943–987.
Ohlmacher, G.C., Aydin, A., 1997. Mechanics of vein, fault and sol-

ution surface formation in the Appalachian Valley and Ridge, northeastern Tennessee, U.S.A.: implications for fault friction, state of stress and fluid pressure. Journal of Structural Geology 19, 927–944.

Palmer, A.C., Rice, J.R., 1973. The growth of slip surfaces in the progressive failure of overconsolidated clay. Proceedings of the Royal Society of London A332, 527–548.

Park, W.C., Schot, E.H., 1968. Stylolites: their origin and nature. Journal of Sedimentary Petrology 38, 175–191.

Peacock, D.C.P., Sanderson, D.J., 1995a. Pull-aparts, shear fractures and pressure solution. Tectonophysics 241, 1–13.

Peacock, D.C.P., Sanderson, D.J., 1995b. Strike-slip relay ramps. Journal of Structural Geology 17, 1351–1360.

Peacock, D.C.P., Fisher, Q.J., Willemse, E.M.J., Aydin, A., 1999. The relationship between faults and pressure solution seams in carbonate rocks and the implications for fluid flow. In: Jones, G., Fisher, Q.J., Knipe, R.J. (Eds.), Faulting, Fault Sealing and Fluid Flow in Hydrocarbon Reservoirs. Geological Society, London, Special Publication 147, pp. 105–115.

Petit, J.P., Barquins, M., 1988. Can natural faults propagate under mode-II conditions? Tectonics 7, 1243–1256.

Petit, J.P., Mattauer, M., 1995. Paleostress superposition deduced from mesoscale structures in limestones: the Matelles exposure, Languedoc, France. Journal of Structural Geology 17, 245–256.

Pollard, D.D., Segall, R.H., 1987. Theoretical displacements and stresses near fractures in rock: with application to faults, joints, veins, dikes, and solution surfaces. In: Atkinson, B.K. (Ed.), Fracture Mechanics of Rock. Academic Press, New York, pp. 227–349.

Reches, Z., Lockner, D.A., 1994. Nucleation and growth of faults in brittle rocks. Journal of Geophysical Research 99, 18159–18173.

Rispoli, R., 1981. Stress fields around strike-slip faults inferred from stylolites and tension gashes. Tectonophysics 75, T29–T36.

Rutter, E.H., 1976. The kinetics of rock deformation by pressure solution. Philosophical Transactions of the Royal Society of London 283, 203–219.

Rutter, E.H., 1983. Pressure solution in nature, theory and experiment. Journal of the Geological Society 140, 725–740.

Salvini, F., Vittori, E., 1982. Analisi strutturale della linea Olevano–Antrodoco–Posta (Ancona–Anzio Auct.): metodologia di studio delle deformazioni fragili e presentazione del tratto meridionale. Memorie della Società Geologica Italiana 24, 337–356.

Salvini, F., 1991a. Considerazioni sull'assetto tettonico crostale lungo il profilo CROP 03 da analisi dei lineamenti telerilevati. Studi Geologici Camerti, volume speciale 1991/1, 99–107.

Salvini, F., 1991b. Tettonica a blocchi in settori crostali superficiali: modellizzazione ed esempi da dati strutturali in Appennino Centrale. Studi Geologici Camerti, volume speciale 1991/2, 237–247.

Salvini, F., 1998. DAISY 2.1 software. Rome.

Sanderson, D.J., Marchini, W.R.D., 1984. Transpression. Journal of Structural Geology 6, 449–458.

Scholz, C.H., Dawers, N.H., Yu, J.-J., Anders, M.H., Cowie, P.A., 1993. Fault growth and fault scaling laws: preliminary results. Journal of Geophysical Research 98, 21951–21961.

Sharpe, D., 1847. On slaty cleavage. Quarterly Journal of the Geological Society 3, 74–105.

Sheldon, P., 1912. Some observations and experiments on joint planes. Journal of Geology 20, 164–183.

Siddans, A.W.B., 1972. Slaty cleavage—A review of research since 1815. Earth Science Review 8, 205–232.

Sorby, H.C., 1853. On the origin of slaty cleavage. Edinburgh New Philosophical Journal 55, 137–148.

Sorby, H.C., 1856. On slaty cleavage as exhibited in the Devonian limestones of Devonshire. Philosophical Magazine 11, 20–37.

Stockdale, P.B., 1922. Stylolites; their nature and origin. Indiana University Studies 9, 1–97.

Vandenberg, J., 1979. Reconstruction of the Western Mediterranean area for the Mesozoic and Tertiary timespan. Geologie en Mijnbouw 58, 153–160.

Weyl, P.K., 1959. Pressure solution and the force of crystallization—A phenomenological theory. Journal of Geophysical Research 64, 2001–2025.

Willemse, E.J.M., Pollard, D.D., 1998. On the orientation and patterns of wing cracks and solution surfaces at the tips of a sliding flaw or fault. Journal of Geophysical Research 103, 2427–2438.

Willemse, E.J.M., Peacock, D.C.P., Aydin, A., 1997. Nucleation and growth of strike-slip faults in limestones from Somerset, UK. Journal of Structural Geology 19, 1461–1477.

Willemse, E.J.M., 1997. Segmented normal faults: correspondence between 3D mechanical models and field data. Journal of Geophysical Research 102, 675–692.

Wise, D.U., McCrory, T.A., 1982. A new method of fracture analysis: azimuth versus traverse distance plots. Geological Society of America Bulletin 93, 889–897.

Wise, D.U., Vincent, R.J., 1965. Rotation axis method for detecting conjugate planes in calcite petrofabric. American Journal of Science 263, 289–301.

Wise, D.U., Funiciello, R., Parotto, M., Salvini, F., 1985. Topographic lineament swarms: Clues to their origin from domain analysis of Italy. Geological Society of America Bulletin 96, 952–967.